AGU PUBLICATIONS

JGR

Journal of Geophysical Research: Space Physics

RESEARCH ARTICLE
10.1002/2014JA020594

Key Points:
- Development of ANN-based TEC models at different longitudes
- Improved performance of TEC models incorporating neutral wind
- Explanation of longitudinal variability of TEC using zonal wind

Correspondence to:
A. Paul,
ashik_paul@rediffmail.com

Citation:
Sur, D., S. Ray, and A. Paul (2015), Role of neutral wind in the performance of artificial neural-network based TEC models at diverse longitudes in the low latitudes, *J. Geophys. Res. Space Physics*, *120*, 2316–2332, doi:10.1002/2014JA020594.

Received 8 SEP 2014
Accepted 17 FEB 2015
Accepted article online 20 FEB 2015
Published online 28 MAR 2015

Role of neutral wind in the performance of artificial neural-network based TEC models at diverse longitudes in the low latitudes

D. Sur[1], S. Ray[1], and A. Paul[1]

[1]Institute of Radio Physics and Electronics, University of Calcutta, Calcutta, India

Abstract The equatorial ionosphere is characterized by (i) large values of total electron content (TEC) and sharp latitudinal gradients of TEC, (ii) steep temporal variation of TEC, (iii) large diurnal variation of TEC, and (iv) postsunset secondary enhancement of TEC. These features cause major limitations in the accuracy of standard ionospheric TEC models in this region. Three artificial neural-network (ANN) based models have been developed based on real-time low-latitude TEC data along 77°E, 88°E, and 121°E longitudes in the region between the magnetic equator and locations beyond the northern crest of equatorial ionization anomaly to predict the vertical TEC values. ANN models have shown more accurate predictions than other standard ionospheric TEC models like International Reference Ionosphere, Parameterized Ionospheric Model, and NeQuick. The effects of the neutral wind in the variation of TEC are significant and have been incorporated as inputs to these ANN models. The outputs with neutral wind incorporated shows better correspondence with measured TEC than the models without neutral wind inputs. The longitudinally separated models have been used to find any longitudinal differences in TEC along equatorial regions. The causes behind the longitudinal differences in TEC and its diurnal variations in these regions have been explained in terms of the geomagnetic declination and inclination angles along with the role of zonal wind.

1. Introduction

Satellite-based communication and navigation systems like GPS (Global Positioning System) and GNSS (Global Navigation Satellite System) propagating through irregularly distributed ionosphere always show amplitude and phase deviations or scintillations. The irregular electron distribution through the ionosphere also causes range error for the GPS signals due to the group delay as the signal is propagating through the perturbing ionosphere. One total electron content (TEC) unit ($1\,\mathrm{TECU} = 10^{16}\,\mathrm{el\,m^{-2}}$) introduces 0.16 m range error at the L1 (1.6 GHz) frequency and 0.27 m range error at the L2 (1.2 GHz) frequency of GPS. The equatorial ionosphere, covering up to 30° geomagnetic dip around the geomagnetic equator, has two very prominent phenomena: (i) the equatorial ionization anomaly (EIA) and (ii) intense electron density irregularities.

At equatorial region, the magnetic field B is very much parallel to the surface of the Earth. The E region electric field E is eastward at daytime. The $E \times B$ force uplifts F region plasma upward at the geomagnetic equator, and this plasma shifts along magnetic field lines. Thus, ionization density at magnetic equator gets reduced, and two crests of EIA formed at 15° to 20° in magnetic north and south having high ionization density. This effect is often called as equatorial ionization anomaly (EIA) or the "fountain effect" [*Appleton*, 1946; *Hanson and Moffett*, 1966]. The fountain rises to several hundred kilometers at the magnetic equator [*Su et al*., 1996].

Due to the large TEC values in the low-latitude regions, all satellite-based augmentation systems (SBAS) are affected by severe ionospheric range delays. The ionospheric TEC causes a group delay in the navigation signal and thus deteriorates the accuracy of the estimated position. Accurate prediction through a TEC model is an essential requirement for low-latitude regions. But theoretical modeling of TEC in this equatorial region is very difficult as the description of TEC variation process is very nonlinear and complex in nature. Midlatitude data-based standard models like International Reference Ionosphere (IRI) and Parameterized Ionospheric Model (PIM) are empirical in nature and unable to produce accurate prediction in the equatorial regions [*Paul et al*., 2005]. So this necessitates the requirement for a model designed by real-time local TEC data for reliable operation of navigation and spacecraft control systems.

The International Reference Ionosphere (IRI) is the most frequently used empirical model for the ionosphere [*Rawer and Bilitza*, 1989, 1990]. Another widely used ionospheric model is the Parameterized Ionospheric Model (PIM) [*Daniell et al*., 1995]. NeQuick is an empirical model and often used to generate electron density profile along height from the satellite to ground receiver along the signal raypath. The necessary inputs for electron density profile computation are altitude of the two ends of raypath, time, month, geographic latitude, longitude, and solar activity indices like sunspot number or 10.7 cm solar radio flux [*di Giovanni and Radicella*, 1990; *Radicella*, 2009]. These empirical models based on midlatitude data always produce smoothed variation of TEC and unable to produce accurate prediction in the equatorial regions [*Paul et al*., 2005; *Bhuyan and Borah*, 2007]. The sharp variable nature of low-latitude TEC cannot be produced by these empirical models, and these models normally show significant deviation from the measured TEC. The equatorial region ionospheric TEC shows steep diurnal, seasonal, latitudinal, as well as longitudinal variations. TEC in equatorial regions has steep diurnal and spatial gradients in both geomagnetically normal and disturbed days [*Klobuchar et al*., 2001; *Paul et al*., 2011]. The daily variability of the location of the EIA peak TEC is very sharp. The change in intensity of EIA is also very dynamic and high in nature in this equatorial region [*Rastogi and Klobuchar*, 1990; *Huang et al*., 1989]. Thus, a real-time TEC data-driven prediction method is required for the equatorial regions.

It is proven that artificial neural network (ANN) approach is very suitable for predicting complex ionospheric parameters [*Altinay et al*., 1997; *Wintoft and Cander*, 1999; *Kumluca et al*., 1999; *McKinnell and Poole*, 2001; *Oyeyemi et al*., 2005a, 2005b, 2006]. Multilayer Perceptron (MLP) technique, has proven to be a standard method to predict complex ionospheric characteristics like the diurnal, seasonal variations of TEC. Some of the models designed to predict the TEC in recent years are reported in *Marquez and Hill* [1992], *Leandro* [2004], *Hernandez-Pajares et al*. [1997], *Tulunay et al*. [2006], *Leandro and Santos* [2007], *Senalp et al*. [2008], and *Yilmaz et al*. [2009].

TEC always undergoes large deviation over different longitudes. The possibility of the presence of longitudinal differences has already been reported in *Su et al*. [1996] and *Zhang et al*. [2011]. In order to inspect any longitudinal difference present over equatorial TEC distribution over time, three real-time ANN-based TEC models along three different longitude regions of 77°E, 88°E, and 121°E for TEC prediction have been developed along low latitudes. They are named as IRPE-TEC-77E, IRPE-TEC-88E, and IRPE-TEC-121E, respectively. The basic blocks of ANN models are artificial neurons. Similar to human brain neuron, these are signal processing and signal transmitting-receiving blocks. MLP is used to train the network as MLP can describe many complex parameters. All the ANN models reported in this paper are designed by the help of feedforward backpropagation architecture. During the feedforward stage of the training period, the inputs are fed forward to the succeeding nodes with properly adjusted weights and biases. After reaching to the output, the calculated value is compared with the desired value. The error of the output is fed back to the input layers in order to adjust the weights and biases in each node. This iteration is repeated several times until the error converges inside a predetermined value. In MLP configuration, the number of layers and the number of neurons in each layer are readjusted by the final performance of the model in different situations. Every model constitutes a training data set in order to make the model learn the relationship between inputs and desired output. The training database of the currently developed ANN models for each longitude constitute real-time GPS data from locations closer to geomagnetic equator to beyond the northern crest of EIA. The initial development of the model IRPE-TEC-88E has been reported in *Sur and Paul* [2013]. The predictions from these models have been compared with the standard models like IRI, PIM, and NeQuick to observe their applicability along low-latitude sector.

The effects of neutral wind components (meridional wind and zonal wind) over TEC have already been reported in literatures [*Fesen et al*., 1989; *Alken et al*., 2008; *Balan et al*., 2009]. In order to inspect the effects of neutral winds over TEC, all the previously mentioned ANN-based models (IRPE-TEC-77E, IRPE-TEC-88E, and IRPE-TEC-121E) have been redesigned with incorporating neutral winds as model inputs. The neutral wind or horizontal wind magnitudes and directions can be obtained from horizontal wind model (HWM07) [*Drob et al*., 2008]. The horizontal wind model (HWM07) provides values of horizontal wind fields of the Earth's atmosphere from the ground to 500 km at the Earth's atmosphere. The model is built by Fortran 90 subroutine, and the data are obtained from over 50 years of satellite- and ground-based wind measurements [*Drob et al*., 2008; *Alken et al*., 2008]. After the introduction of neutral winds as inputs to the models, the newly designed models along 77°E, 88°E, and 121°E longitudes have been renamed as

Table 1. GPS-TEC Data Receiver Stations for Training and Simulation Data Set for IRPE-TEC-88E

Station Name	Geographic Latitude (°N)	Geographic Longitude (°E)	Geomagnetic Dip (°N)	Training Data Period	Simulation Data Period
Calcutta	22.58	88.38	32	1 January 2007 through 15 September 2011	October 2011 and April 2012
Baharmpore	24.09	88.25	35	23 March 2011 through 15 September 2011	October 2011
Farakka	24.79	87.89	36	Data set from Farakka is not used for model training	April 2012
Siliguri	26.72	88.39	40	1–15 September 2011	April 2012

IRPE-TEC-77E(HWM), IRPE-TEC-88E(HWM), and IRPE-TEC-121E(HWM), respectively. The predictions from these wind-incorporated ANN models have been compared with the models without neutral wind components as inputs (IRPE-TEC-77E, IRPE-TEC-88E, and IRPE-TEC-121E) and also with the standard models like IRI, NeQuick, and PIM.

The final objective of the paper is to observe any longitudinal difference in TEC distribution along different longitudes. Any longitudinal differences except the differences due to solar terminator have been observed and quantified. The currently developed ANN models have been used to inspect the longitudinal TEC differences, and this longitudinal difference pattern has also been inspected for any diurnal variation in this paper.

2. Development and Performance Analysis of a Neural Network-Based TEC Model Along 88°E

An ANN-based TEC model, IRPE-TEC-88E, has been designed along 88°E longitude with real-time GPS-TEC data obtained from the stations mentioned in Table 1. The locations of these stations are shown in Figure 1a. The GPS-TEC data are obtained at Calcutta from a dual-frequency Ionospheric Scintillation and TEC Monitor. This dual-frequency GPS receiver is operational under Institute of Radio Physics and Electronics (IRPE), University of Calcutta, since November 2006 as a part of SCINDA (SCIntillation Network Decision Aid) program. GPS-TEC data at Baharampore are obtained from another dual-frequency Ionospheric Scintillation and TEC Monitor at K. N. College, Baharampore. At Siliguri, the GPS-TEC data are recorded from software-based dual-frequency GPS TEC recorder at North Bengal University, Siliguri. The processed TEC data from Calcutta can be accessed by authorized users from the website http://capricorn.bc.edu/scinda/india. The entire training period is mentioned in Table 1. Only geomagnetically quiet days ($Dst \geq -50$ nT) are selected for training the model. The initial development of this model has been reported in *Sur and Paul* [2013]. The data set for this model extends along 88°E subionospheric longitude covering a wide subionospheric latitude span of 20°–28°N from EIA crest to beyond the northern crest of EIA. This data set period covers low to moderate solar activity period of 23rd solar cycle. At these three stations, slant TEC (STEC) data have been monitored and recorded with a 1 min resolution.

Slant TEC (STEC) recorded from those stations for an elevation angle greater than 50° is used as training data set for model IRPE-TEC-88E. STEC obtained from below elevation angle 50° has been excluded in order to avoid the local time effects. The equivalent vertical TEC (VTEC) has been obtained from STEC by equations (1) and (2) shown below.

$$\text{Slanting Factor} = 1/\left\{\left[1 - r\text{Cos}\,E/\,(r+I)^2\right]^{1/2}\right\}, \quad (1)$$

$$\text{VTEC} = \text{STEC}/\,\text{Slanting Factor}. \quad (2)$$

All TEC values are expressed in TECU (1 TECU = 10^{16} el/m^2) in this paper.
r the radius of the Earth, meter.
E the elevation angle for the receiver location, degree.
I the height of the maximum electron density, normally considered to be at height of 350 km, meter [*Breed et al.*, 1997; *Nava et al.*, 2007].

The conversion function between VTEC and STEC is shown in equation (2). These VTEC conversion methods shown in equations (1) and (2) have been reported in *Sur and Paul* [2013]. The inputs for the model are

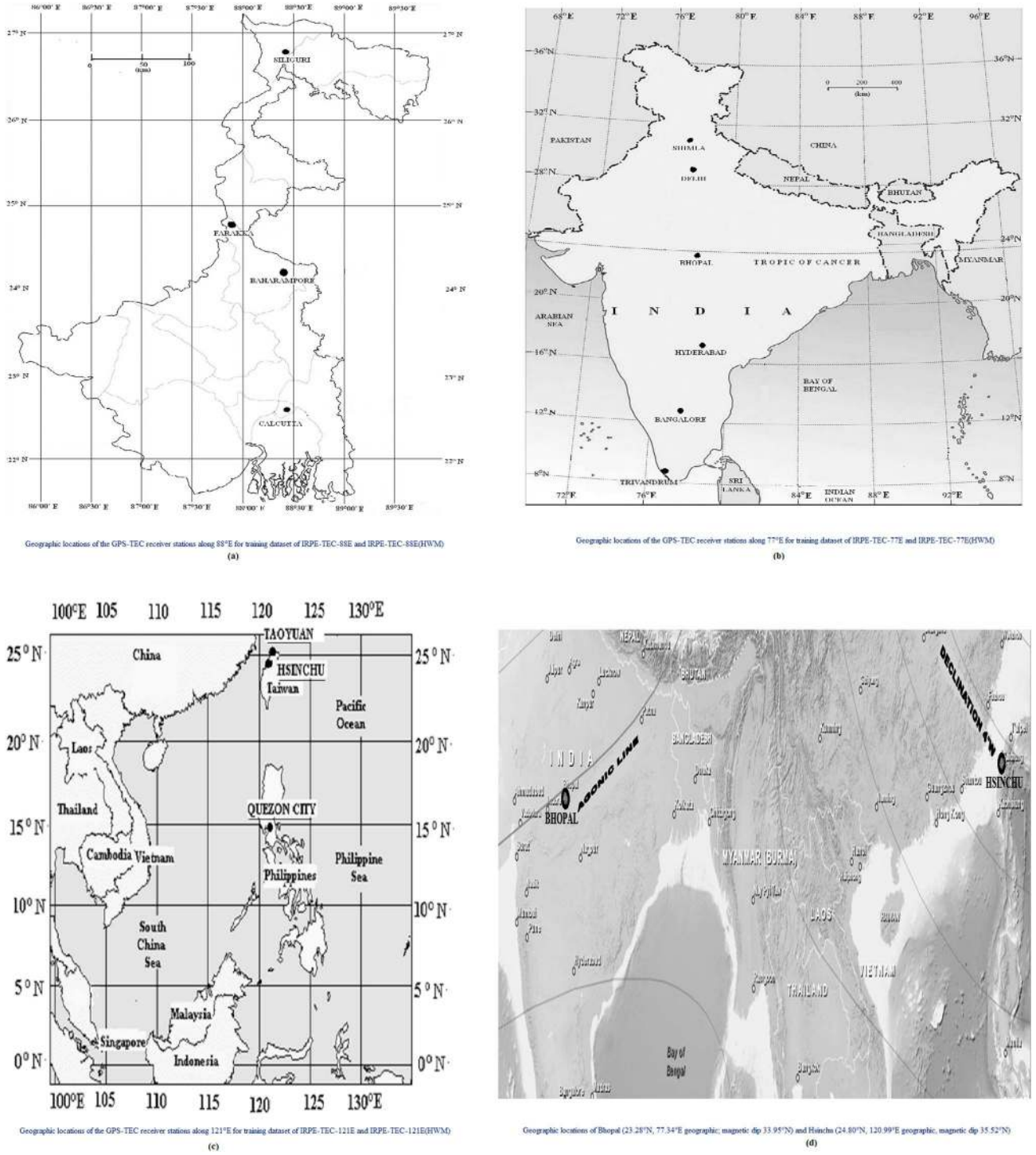

Figure 1. (a) Geographic locations of the GPS-TEC receiver stations along 88°E for training data set of IRPE-TEC-88E and IRPE-TEC-88E(HWM). (b) Geographic locations of the GPS-TEC receiver stations along 77°E for training data set of IRPE-TEC-77E and IRPE-TEC-77E(HWM). (c) Geographic locations of the GPS-TEC receiver stations along 121°E for training data set of IRPE-TEC-121E and IRPE-TEC-121E(HWM). (d) Geographic locations of Bhopal (23.28°N, 77.34°E geographic, magnetic dip 33.95°N) and Hsinchu (24.80°N, 120.99°E geographic, magnetic dip 35.52°N).

sequentially ordered by (i) day of year, (ii) time in UT, (iii) 350 km subionospheric latitude, (iv) 350 km subionospheric longitude, and (v) daily sunspot number. Geomagnetically disturbed conditions are filtered out by selecting days only with $Dst \geq -50$ nT for model designing. The model produces vertical TEC at a 1 min resolution.

Predicted TEC from this model (IRPE-TEC-88E) has also been compared with the TEC obtained from globally accepted TEC models like IRI and PIM for the two equinoxes, October 2011 and April 2012. The simulation data set is completely different from the training data set in order to avoid biasing. The GPS-TEC receiver stations, which have been used for simulation purpose, are shown in Table. 1. The simulation is performed only for geomagnetically quiet days ($Dst \geq -50$ nT). The locations of those stations are shown in Figure 1a.

3. Incorporation of Neutral Wind as Inputs to the TEC Model

It has been established that the TEC is also dependent on horizontal neutral wind flow and velocity of its major components like meridional wind and zonal wind [*Fesen et al*., 1989; *Alken et al*., 2008; *Balan et al*., 2009]. Horizontal neutral winds have a strong effect in equatorial *E* and *F* region ionospheric parameters [*Alken et al*., 2008]. A penetrating eastward electric field coupled with equatorward neutral wind strengthens the day time EIA and produces a super plasma fountain [*Kelley et al*., 2004], which drives the plasma upward causing less ion recombination and higher value of TEC in the low-latitude equatorial region. The upwelling of the plasma at the equatorial region causes reduction to poleward plasma flow. The direct effect of neutral wind without penetrating eastward electric field over TEC has also been established [*Balan et al*., 2009]. Equatorward neutral wind elevates the ionosphere to very high altitude in the low-latitude regions, preventing it to be lost by chemical recombination and chemical diffusion due to gravity. Due to the dependence of TEC over the components of neutral winds, the model IRPE-TEC-88E has been modified with the incorporation of meridional wind and zonal wind as model inputs. The meridional wind and zonal wind velocities are obtained from horizontal wind model (HWM07) [*Drob et al*., 2008]. These neutral wind values are fed to IRPE-TEC-88E as model inputs, and this wind-incorporated ANN model has been renamed as IRPE-TEC-88E(HWM). The data set for IRPE-TEC-88E(HWM) is real-time TEC data from GPS-TEC receiver stations for the training data set period shown in Table 1. After addition of two neutral wind inputs, the seven inputs of IRPE-TEC-88E(HWM) are now sequentially (i) day of year, (ii) time in UT, (iii) 350 km subionospheric latitude, (iv) 350 km subionospheric longitude, (v) daily sunspot number, (vi) meridional wind, and (vii) zonal wind. Only geomagnetically quiet days ($Dst \geq -50$ nT) are considered in training data set alongside only TEC over elevation angle of 50° is used to avoid local time effects. This model produces vertical TEC at a 1 min interval.

The wind-incorporated ANN model (IRPE-TEC-88E(HWM)) is tested for a series of simulation for the period of April 2012 for geomagnetically quiet days ($Dst \geq -50$ nT) from the stations (i) Calcutta (22.58°N, 88.38°E geographic, magnetic dip 32°N), (ii) Siliguri (26.72°N, 88.39°E geographic, magnetic dip 40°N), and (iii) Farakka (24.79°N, 87.89°E geographic, magnetic dip 36°N) and compared with the prediction from other models. The equatorial ionosphere is responsive to seasonal variations with highest perturbations in ionization/TEC noted during the equinoctial months. Accordingly, April 2012 has been selected for comparison as it presents one of the worst case scenarios. However, similar analyses spanning more extended period may provide further details. In fact, validation of the functions used in developing the ANN could be more extensive when tested over more exhaustive time lines. Further, the present manuscript reports validation of ANN-based TEC models developed at 88°E in comparison to other standard ionospheric models like IRI, PIM, and NeQuick. Data for the ANN model were generated by operating GPS receivers at stations near and beyond the northern crest of EIA on campaign mode. Because of the resource-crunching nature of the campaigns, data beyond the period reported in this paper are not available from all the stations. For April 2012, the simulation data set is completely different from the training data set in order to avoid biasing. Figure 2a shows the comparisons from one representative geomagnetically quiet day 28 April 2012 from entire simulation period of April 2012 at the Calcutta station (22.58°N, 88.38°E geographic, magnetic dip 32°N). The Calcutta station lies on the crest of EIA. The performance of neutral wind coupled model IRPE-TEC-88E(HWM) has been improved almost throughout the day, especially from diurnal peak and the later phase of the day. The predicted TEC of PIM, NeQuick, and IRI have shown significant deviation from the actual VTEC at diurnal peak. PIM overestimates TEC near the diurnal peak. The predictions of IRI, NeQuick, and PIM have shown slightly better correspondence with actual VTEC at 20:00–23:00 UT and 00:00–02:00 UT. On that particular representative geomagnetically quiet day (28 April 2012), TEC prediction deviations shown by the models IRPE-TEC-88E, PIM, IRPE-TEC-88E(HWM), NeQuick, and IRI at diurnal peak TEC are tabulated in Table 2.

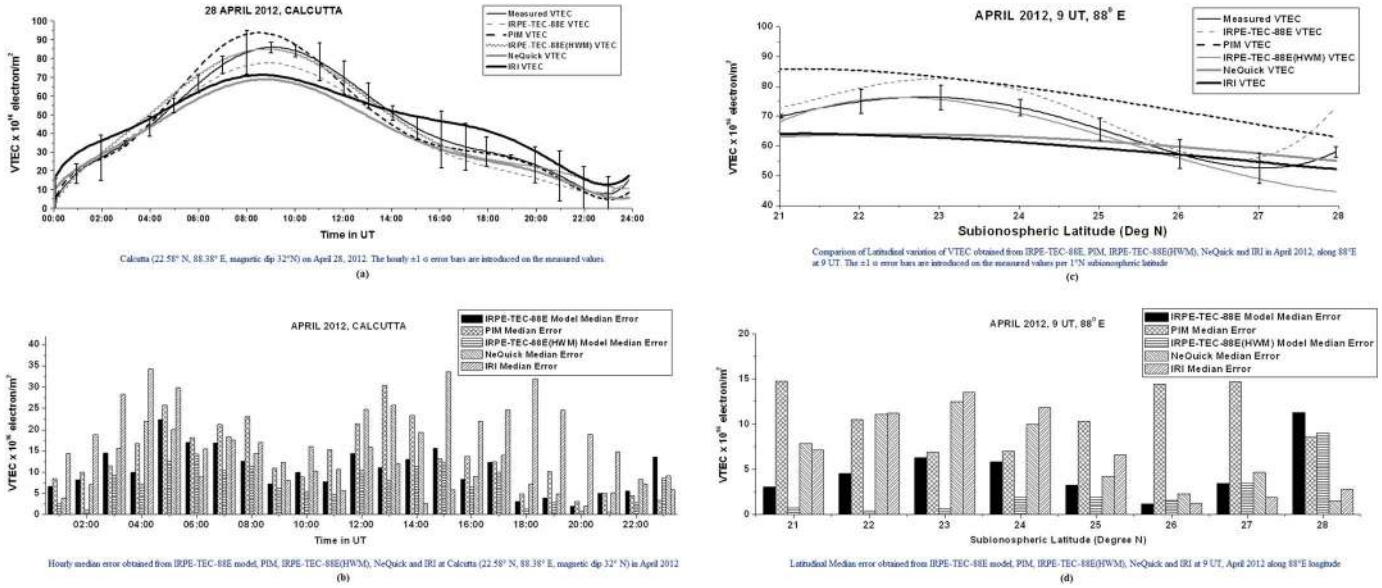

Figure 2. (a) Comparison of diurnal variation of actual VTEC with VTEC obtained from IRPE-TEC-88E, PIM, IRPE-TEC-88E(HWM), NeQuick, and IRI at Calcutta (22.58°N, 88.38°E, magnetic dip 32°N) on 28 April 2012. The hourly ±1σ error bars are introduced on the measured values. (b) Hourly median error obtained from IRPE-TEC-88E model, PIM, IRPE-TEC-88E(HWM), NeQuick, and IRI at Calcutta (22.58°N, 88.38°E, magnetic dip 32°N) in April 2012. (c) Comparison of latitudinal variation of VTEC obtained from IRPE-TEC-88E, PIM, IRPE-TEC-88E(HWM), NeQuick, and IRI in April 2012 along 88°E at 09:00 UT. The ±1σ error bars are introduced on the measured values per 1°N subionospheric latitude. (d) Latitudinal median errors obtained from IRPE-TEC-88E model, PIM, IRPE-TEC-88E(HWM), NeQuick, and IRI at 09:00 UT in April 2012 along 88°E longitude.

The similar comparisons have been done for all the geomagnetically quiet days from April 2012. Combining those data over the whole month of April 2012, hourly median prediction errors have been computed from IRPE-TEC-88E, PIM, IRPE-TEC-88E(HWM), NeQuick, and IRI, and those results have been shown in Figure 2b.

The deviations of predicted VTEC for IRPE-TEC-88E, PIM, IRPE-TEC-88E(HWM), NeQuick, and IRI from actual VTEC have been quantified in diurnal basis. Figure 2b shows the hourly median error for each hour from April 2012 (for geomagnetically quiet days) from IRPE-TEC-88E, PIM, IRPE-TEC-88E(HWM), NeQuick, and IRI in diurnal basis from the EIA crest station Calcutta for elevation angle greater than 50°. The measured TEC from elevation angle below 50° has not been chosen to avoid local time effects. From the analysis, it can be observed that all the models have shown significant amount of deviations at the diurnal peak from the actual VTEC, while IRPE-TEC-88E(HWM) shows the minimum error at diurnal peak and PIM and NeQuick show large deviation from the actual VTEC. The incorporation of neutral winds as model inputs significantly reduces the TEC prediction deviation from actual VTEC almost throughout the day. The maximum median errors from the actual VTEC obtained from the models IRPE-TEC-88E, PIM, IRPE-TEC-88E(HWM), NeQuick, and IRI are shown in Table 2. The corresponding universal time is shown in brackets after the median TEC values. The median errors obtained by all models at diurnal peak for April 2012 at Calcutta are also tabulated in Table 2.

Table 2. Diurnal and Latitudinal Performance Comparison for Models Along 88°E in April 2012

Diurnal Performance Analysis for Models Along 88°E in April 2012 at Calcutta					
	IRPE-TEC-88E (TECU)	PIM (TECU)	IRPE-TEC-88E(HWM) (TECU)	NeQuick (TECU)	IRI (TECU)
Error TEC at diurnal peak on 28 April 2012	8	9	1	17	14
Maximum median prediction error in the entire April 2012	22 (5 UT)	30 (13 UT)	14 (6 UT)	34 (15 UT)	34 (4 UT)
Median error TEC at diurnal peak in the entire April 2012	7	10	6	12	8
Latitudinal Performance Analysis for Models Along 88°E in April 2012 for Latitude Span of 21°N–28°N					
	IRPE-TEC-88E (TECU)	PIM (TECU)	IRPE-TEC-88E(HWM) (TECU)	NeQuick (TECU)	IRI (TECU)
Maximum median prediction error for latitude span of 21°N–28°N in the entire April 2012	11 (28°N)	15 (21°N)	10 (28°N)	12 (23°N)	13 (23°N)
Prediction error at EIA crest in the entire April 2012	6.3	6.9	0.66	12	13

A latitudinal TEC variation comparison has also been done for actual VTEC and VTEC obtained from IRPE-TEC-88E, PIM, IRPE-TEC-88E(HWM), NeQuick, and IRI for all the geomagnetic quiet days of equinoctial month April 2012 from a fixed subionospheric longitude of 88°E at 09:00 UT covering latitudinal swath of 21°N to 28°N. The actual VTEC having elevation angle over 50° is only considered for this comparison in order to avoid local time effects. The comparisons are shown in Figure 2c. From the comparison, it can be concluded that neutral wind-incorporated ANN model IRPE-TEC-88E(HWM) shows better correspondence with actual VTEC than the other models. IRI and NeQuick have shown less sensitivity toward the latitudinal variation of actual VTEC, and these models have shown large TEC deviation from the actual VTEC. PIM overestimates TEC values along the entire latitudinal span. The TEC deviations of predicted VTEC of IRPE-TEC-88E, PIM, IRPE-TEC-88E(HWM), NeQuick, and IRI from actual VTEC have been observed in latitudinal basis. Figure 2d shows the monthly median error analysis from the month of April 2012 (for geomagnetically quiet days) from IRPE-TEC-88E, PIM, IRPE-TEC-88E(HWM), NeQuick, and IRI with latitude variation for fixed longitude of 88°E for 09:00 UT. From the analysis, it can be observed that all the models have shown significant amount of deviations at EIA crest from the actual VTEC except IRPE-TEC-88E(HWM). IRPE-TEC-88E(HWM) has shown the minimum error at EIA crest. IRI and NeQuick show large deviations from the actual VTEC at EIA crest. IRPE-TEC-88E(HWM) has shown less median error almost throughout the latitudinal span of 21°N–28°N, justifying the incorporation of neutral winds as model inputs. The maximum median errors obtained from IRPE-TEC-88E, PIM, IRPE-TEC-88E(HWM), NeQuick, and IRI are summarized in Table 2. The corresponding latitude is also shown in brackets after the median TEC value. At EIA crest, the median TEC prediction errors for IRPE-TEC-88E, PIM, IRPE-TEC-88E(HWM), NeQuick, and IRI for entire month of April 2012 are shown in Table 2.

4. Longitudinal Variation of TEC

From the study made by *Su et al.* [1996] using the Sheffield University plasmasphere-ionosphere model with the observations from Hinotori satellite, operated with an orbit at an altitude of about 600 km, it has been established that low-latitude ionosphere suffers longitudinal variations due to the variations of neutral wind, $E \times B$ drift velocities, and the displacements of geomagnetic declination angle. Thus, the longitudinal variation of TEC can be attributed to the variation of geomagnetic declination angle and the zonal wind. The magnetic field-aligned ion drift velocity V (conventionally positive for upward drift) due to thermospheric horizontal zonal winds Z (positive for eastward winds) can be related by equation (3).

$$V = -Z \sin \mathrm{Dec} \cos \mathrm{Inc} \quad [\textit{Zhang et. al.}, 2011] \tag{3}$$

V geomagnetic field-aligned ion drift velocity (positive for upward drift), m/s.
Z zonal wind velocity (positive for eastward winds), m/s.
Inc the geomagnetic inclination (positive for northern angle), degree.
Dec the geomagnetic declination (positive for east angle), degree.
V is either upward or downward depending on the sign of declination angle Dec and the sign of zonal winds Z.

For a westward directed wind, V becomes downward for west or negative declination angle and upward for east or positive declination angle for north inclination angle. If V becomes downward, it moves the ions to lower altitudes, and this increases their recombination rate, which is also exponentially increasing at the lower altitudes. Thus, TEC gets decreased. On the other hand, the upward drift of V would increase the TEC as it moves the plasma to the higher altitudes causing less recombination rate. In these regions, high TEC values can be obtained. The direction of zonal wind varies from eastward to westward in diurnal basis. According to model HWM07, at Hsinchu (24.80°N, 120.99°E geographic, magnetic dip 35.52°N), the directions of the zonal wind become eastward through the morning hours in daytime and become westward from the local noontime to nighttime (shown in Figures 5e and 5f). This variation coupled with the declination angle of the station provides the variation of TEC in different longitude regions.

To observe the longitudinal differences that may occur in the variation of TEC except variation due to solar terminator, two ANN-based TEC models have been designed along 77°E and 121°E longitude at the equatorial low-latitude regions. These models are named as IRPE-TEC-77E and IRPE-TEC-121E, respectively. The inputs for those models are (i) day of year, (ii) time in UT, (iii) 350 km subionospheric latitude, (iv) 350 km subionospheric longitude, and (v) daily sunspot number. Only geomagnetically quiet days ($Dst \geq -50$ nT) are selected among the database. These models have been redesigned with the incorporation of neural wind components (the magnitude and directions of meridional wind and zonal wind) obtained from HWM07

Table 3. GPS-TEC Data Receiver Stations for Training Data Set for IRPE-TEC-77E and IRPE-TEC-77E(HWM) and Diurnal and Latitudinal Performance Comparison for Models Along 77°E in April 2005

Station Name	Geographic Latitude (°N)	Geographic Longitude (°E)	Geomagnetic Dip (°N)	Training Data Period	Simulation Period
Trivandrum	8.47	76.91	0.9		
Bangalore	12.95	77.68	11.69	January 2004 to March 2005	April 2005
Hyderabad	17.44	78.47	21.9		
Bhopal	23.28	77.34	33.95		
Delhi	28.58	77.21	43.5		
Shimla	31.09	77.07	47.43		
Diurnal Performance Analysis for Models Along 77°E in April 2005					
	IRPE-TEC-77E (TECU)	PIM (TECU)	IRPE-TEC-77E(HWM) (TECU)	NeQuick (TECU)	IRI (TECU)
Error TEC at diurnal peak on 9 April 2005 from Hyderabad	1.21	6	0.06	12	11
Maximum median prediction error in entire April 2005 from Bhopal	12 (00:00 UT)	16 (01:00 UT)	9 (02:00 UT)	24 (12:00 UT)	22 (07:00 UT)
Median error TEC at diurnal peak in entire April 2005 from Bhopal	5	10	4	15	14
Latitudinal Performance Analysis for Models Along 77°E in April 2005 for Latitude Span of 8°N–31°N					
	IRPE-TEC-77E (TECU)	PIM (TECU)	IRPE-TEC-77E(HWM) (TECU)	NeQuick (TECU)	IRI (TECU)
Maximum median prediction error for latitude span of 8°–31°N in the entire April 2005	14 (31°N)	31 (31°N)	10 (27°N)	27 (31°N)	26 (31°N)
Prediction error at EIA crest in the entire April 2005	4	5	2	16	17

model as their inputs. The wind-incorporated ANN models along 77°E and 121°E have been renamed as IRPE-TEC-77E(HWM) and IRPE-TEC-121E(HWM), respectively. Seven inputs for these models are (i) day of year, (ii) time in UT, (iii) 350 km subionospheric latitude, (iv) 350 km subionospheric longitude, (v) daily sunspot number, (vi) meridional wind, and (vii) zonal wind. VTEC over 50° elevation is considered for the data set of those models in order to avoid the effects of local time. Only geomagnetically quiet days are considered for training data set. These models generate vertical TEC with a 1 min time resolution. The predictions from wind-incorporated ANN models have been again tested with a series of simulation for equinoctial periods and compared between the models before and after the inclusion of neutral winds as well as with standard TEC models like NeQuick, PIM, and IRI. Simulation data set and training data set for these two models are maintained differently to avoid biasing. This study will help to find out the effects of neutral wind over the variation of TEC. IRPE-TEC-77E(HWM) and IRPE-TEC-121E(HWM) models will also be used to observe the longitudinal TEC differences between 77°E and 121°E longitudes. Any diurnal variation of these longitudinal TEC difference have been studied and reported in section 7 of the present paper.

5. Development and Performance Analysis of a Neural Network-Based TEC Model Along 77°E

The model IRPE-TEC-77E has been designed with the real-time GPS database obtained from a chain of six GAGAN (GPS-Aided Geo-Augmented Navigation) stations situated more or less around 77°E longitude and distributed along the region from geomagnetic equator through the northern crest of EIA to regions beyond the northern crest of EIA. This wide latitudinal variation (8°N–31°N) will be helpful to analyze latitudinal variation of TEC over a fixed longitude. The six GAGAN stations from where the data set is received from January 2004 to March 2005 are shown in Table 3 as well as in Figure 1b.

The data set of IRPE-TEC-77E includes geomagnetically quiet days (days with $Dst \geq -50$ nT) only. TEC below 50° elevation has been excluded to eliminate local time effects. The model inputs are (i) day of year, (ii) time in UT, (iii) 350 km subionospheric latitude, (iv) 350 km subionospheric longitude, and (v) daily sunspot number. In the next step, IRPE-TEC-77E model has been further redesigned with the inclusion of neutral wind components as the model inputs. The wind-incorporated ANN-based model has been renamed as IRPE-TEC-77E(HWM). The magnitudes and directions of neutral wind components like meridional wind and

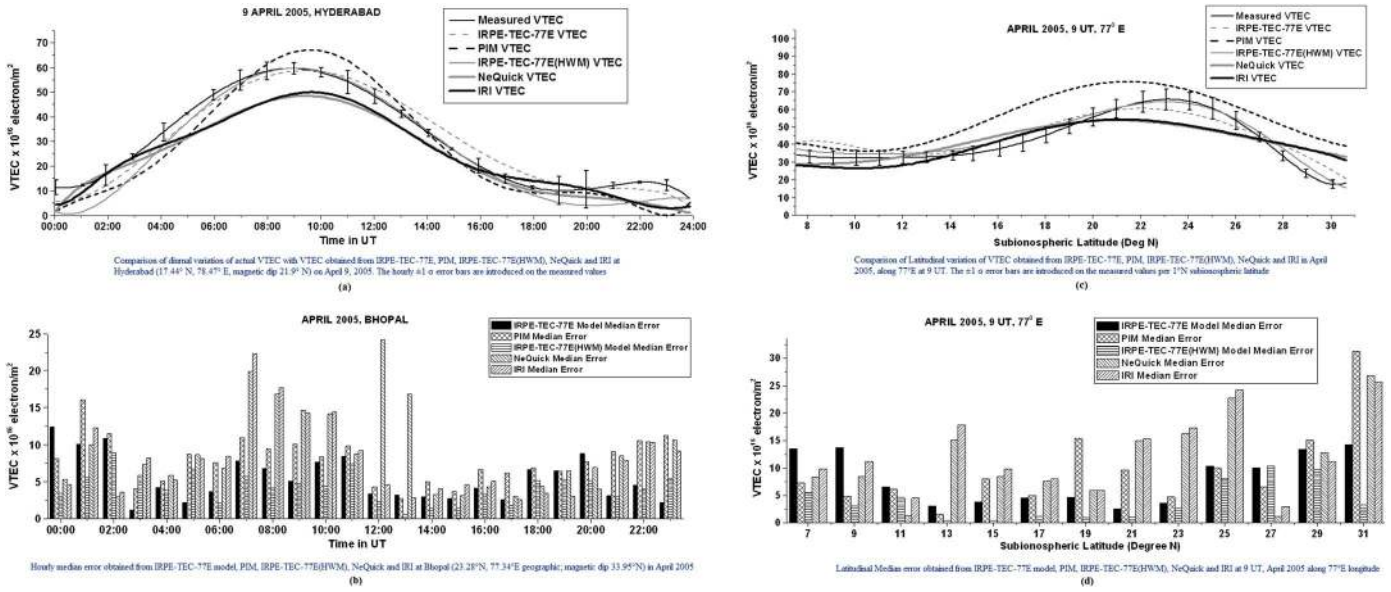

Figure 3. (a). Comparison of diurnal variation of actual VTEC with VTEC obtained from IRPE-TEC-77E, PIM, IRPE-TEC-77E(HWM), NeQuick, and IRI at Hyderabad (17.44°N, 78.47°E, magnetic dip 21.9°N) on 9 April 2005. The hourly ±1σ error bars are introduced on the measured values. (b) Hourly median error obtained from IRPE-TEC-77E model, PIM, IRPE-TEC-77E(HWM), NeQuick, and IRI at Bhopal (23.28°N, 77.34°E geographic, magnetic dip 33.95°N) in April 2005. (c) Comparison of latitudinal variation of VTEC obtained from IRPE-TEC-77E, PIM, IRPE-TEC-77E(HWM), NeQuick, and IRI in April 2005 along 77°E at 09:00 UT. The ±1σ error bars are introduced on the measured values per 1°N subionospheric latitude. (d) Latitudinal median error obtained from IRPE-TEC-77E model, PIM, IRPE-TEC-77E(HWM), NeQuick, and IRI at 09:00 UT in April 2005 along 77°E longitude.

zonal wind have been obtained from HWM07 model [*Drob et al*., 2008]. The training data set for this model is the same as IRPE-TEC-77E. The inputs for IRPE-TEC-77E(HWM) are (i) day of year, (ii) time in UT, (iii) 350 km subionospheric latitude, (iv) 350 km subionospheric longitude, (v) daily sunspot number, (vi) meridional wind, and (vii) zonal wind. Days with $Dst \geq -50$ nT are only considered for designing both ANN models. The TEC obtained from below elevation angle of 50° has been excluded from training data set to avoid local time effects. IRPE-TEC-77E and IRPE-TEC-77E(HWM) produce VTEC at a 1 min resolution. The predictions from both these models have been compared with predictions obtained from NeQuick, PIM, and IRI for the low solar activity vernal equinox period of April 2005 for geomagnetically quiet days (days with $Dst \geq -50$ nT). The ANN model along 77°E, which was designed without the components of neutral wind as model inputs (IRPE-TEC-77E), has also been compared with IRPE-TEC-77E(HWM) to conclude the overall effects of neutral wind toward TEC. The simulation data set is obtained from those six GAGAN stations mentioned in Table 3. However, the simulation data set is deliberately chosen from different time periods from training data set time periods to avoid biasing. The comparisons from 9 April 2005 have been shown as one representative geomagnetically quiet day from the entire simulation month of April 2005 at Figure 3a from the Hyderabad station (17.44°N, 78.47°E geographic, magnetic dip 21.9°N), which is situated to the south from the EIA crest. From the comparison, it can be concluded that while the neutral wind components are included as model inputs, the performance of the model has been improved significantly especially around diurnal peak. However, ANN model without neutral wind shows better correspondence with actual VTEC before 04:00 UT and after 18:00 UT. IRPE-TEC-77E(HWM) has shown minimum deviation from actual VTEC at diurnal peak with the deviation of 0.06 TECU from actual VTEC, while IRPE-TEC-77E, PIM, NeQuick, and IRI have shown TEC deviation of 1.21, 6, 12, and 11 TECU, respectively, from actual VTEC. Both ANN-based models have shown less TEC deviations than PIM, NeQuick, and IRI almost throughout the day especially at diurnal peak. The results are summarized in Table 3. Similar comparisons have been done for the other geomagnetically quiet days of April 2005. Combining those prediction values over all the geomagnetically quiet days from April 2005, the monthly median TEC prediction errors have been computed from IRPE-TEC-77E, PIM, IRPE-TEC-77E(HWM), NeQuick, and IRI, and those results have been shown in Table 3 and Figure 3b.

Figure 3b shows the diurnal variation of median error per hour from IRPE-TEC-77E, PIM, IRPE-TEC-77E(HWM), NeQuick, and IRI along the crest station Bhopal (23.28°N, 77.34°E geographic, magnetic dip 33.95°N) from

April 2005 for elevation angle over 50° for geomagnetic quiet days. From Figure 3b, it can be demonstrated that NeQuick, IRI, and PIM show significant amount of deviations during diurnal peak, while IRPE-TEC-77E(HWM) shows the minimum error among all the models almost throughout the day. The TEC prediction error for PIM has been slightly reduced at diurnal peak. The maximum median errors evaluated from IRPE-TEC-77E, PIM, IRPE-TEC-77E(HWM), NeQuick, and IRI are tabulated in Table 3. The corresponding universal time is also provided in brackets after the median TEC value. The median errors obtained from all models at diurnal peak for April 2005 at Bhopal are also tabulated in Table 3.

The latitudinal variation of the actual VTEC along the fixed 77°E longitude has also been compared with the predictions from IRPE-TEC-77E, IRPE-TEC-77E(HWM), PIM, NeQuick, and IRI to see the effectiveness of those models for predicting the dynamic and wide latitudinal variation of VTEC. The VTEC predictions from IRPE-TEC-77E, IRPE-TEC-77E(HWM), PIM, NeQuick, and IRI along the vast latitudinal range of 8°N–31°N have been compared with the actual VTEC for observing the applicability of those models to describe the latitudinal signature of VTEC at 09:00 UT along fixed longitude 77°E for geomagnetic quiet days of April 2005 for elevation angle over 50°. The comparison is shown in Figure 3c. From the comparison, it can be addressed that the incorporation of neutral wind as model input has increased the sensitivity of the model for predicting the latitudinal variation of VTEC over the latitudinal span starting from the equator to the region beyond the northern crest of EIA. IRPE-TEC-77E(HWM) predicts better than IRPE-TEC-77E almost throughout the entire selected latitudinal span. PIM, NeQuick, and IRI are less sensitive to the latitudinal variation of VTEC. NeQuick and IRI are least sensitive to the latitudinal variation of VTEC. PIM overestimates TEC values at EIA crest. NeQuick and IRI underestimate TEC values at the same region. The median of the deviations of predicted VTEC for IRPE-TEC-77E, PIM, IRPE-TEC-77E(HWM), NeQuick, and IRI models from actual VTEC has been computed along latitudinal basis. The median errors or deviations for all geomagnetic quiet days of April 2005 have been computed and displayed in Figure 3d for wide variation of latitudes during a fixed time interval of 09:00 UT along a fixed longitude of 77°E with an elevation angle over 50°. From Figure 3d, it has been established that NeQuick and IRI models are least sensitive toward the latitudinal variation of the VTEC and have shown large deviations from the actual VTEC. IRPE-TEC-77E(HWM) shows improvement in predicting the VTEC over IRPE-TEC-77E almost throughout the latitude distribution especially at the northern crest of EIA. The maximum median errors obtained from IRPE-TEC-77E, PIM, IRPE-TEC-77E(HWM), NeQuick, and IRI during entire subionospheric latitude range for April 2005 are recorded in Table 3. The corresponding latitudes are also shown in brackets after the median TEC values. At the northern crest of EIA, the TEC median prediction errors occurred from IRPE-TEC-77E, PIM, IRPE-TEC-77E(HWM), NeQuick, and IRI are also tabulated in Table 3. From these comparisons, it can be concluded that IRPE-TEC-77E(HWM) has shown least TEC prediction error at the northern crest of EIA and almost throughout the entire latitudinal span of 8°N–31°N along fixed longitude 77°E for April 2005.

6. Development and Performance Analysis of a Neural Network-Based TEC Model Along 121°E

In order to observe any longitudinal variation of VTEC present in low latitudes, an ANN-based TEC model, IRPE-TEC-121E, has been designed along 121°E longitude by combining the real-time GPS data obtained from the IGS (International GNSS Service) stations along the equatorial region. The data have been processed by a software developed by Gopi Seemala from the Institute for Scientific Research, Boston College, USA [*Seemala and Valladares*, 2011]. Training databases for the models are obtained from the GPS-TEC receiver stations mentioned in Table 4. The locations of these stations are shown in Figure 1c.

This model consists of the data set from only geomagnetically quiet days (days with $Dst \geq -50$ nT). The inputs of the model are (i) day of year, (ii) time in UT, (iii) 350 km subionospheric latitude, (iv) 350 km subionospheric longitude, and (v) daily sunspot number. It also produces vertical TEC at a 1 min interval. TEC data set of an elevation angle over 50° elevation is used in order to avoid local time effects. This model is also redesigned with the inclusion of magnitudes and directions of the components of neutral wind such as meridional wind and zonal wind and is renamed as IRPE-TEC-121E(HWM). The data set for IRPE-TEC-121E(HWM) is the same as IRPE-TEC-121E. IRPE-TEC-121E(HWM) data set only includes geomagnetically quiet days (days with $Dst \geq -50$ nT) with TEC over an elevation angle 50° to reduce the local time effects. The magnitudes and directions of neutral winds are obtained from HWM07 model. The inputs of IRPE-TEC-121E(HWM) are (i) day of year, (ii) time

Table 4. GPS-TEC Data Receiver Stations for Training Data Set for IRPE-TEC-121E and IRPE-TEC-121E(HWM) and Diurnal Performance Analysis for Models Along 121°E in September 2013 at Hsinchu

GPS-TEC data receiver stations for training dataset for IRPE-TEC-121E and IRPE-TEC-121E(HWM)					
Station Name	Geographic Latitude (°N)	Geographic Longitude (°E)	Geomagnetic Dip (°N)	Training Data Period	Simulation Data Set
Hsinchu	24.80	120.99	35.52	January 2011 to March 2012	April 2012, September 2012, April 2013, and September 2013
Taoyuan	24.95	121.16	35.76		
Quezon City	14.64	121.08	15.50		

Diurnal Performance Analysis for Models Along 121°E in September 2013 at Hsinchu					
	IRPE-TEC-121E (TECU)	PIM (TECU)	IRPE-TEC-121E(HWM) (TECU)	NeQuick (TECU)	IRI (TECU)
Error TEC at diurnal peak on 7 September 2013	0.3	5	2	4	16
Maximum median prediction error in the entire September 2013	21 (10:00 UT)	27 (03:00 UT)	8 (10:00 UT)	20 (09:00 UT)	22 (10:00 UT)
Median error TEC at diurnal peak in entire September 2013	6	6	4	7	7

in UT, (iii) 350 km subionospheric latitude, (iv) 350 km subionospheric longitude, (v) daily sunspot number, (vi) meridional wind, and (vii) zonal wind. The applicability of the model has been visualized by a series of simulations for the months of April and September 2012 and April and September 2013 for geomagnetically quiet days. This model IRPE-TEC-121E(HWM) is also compared with IRPE-TEC-121E to see the effects of neutral wind over TEC. The predictions from standard models like PIM, NeQuick, and IRI are also compared with the currently designed ANN models. The simulation data set is deliberately kept different from the training data set in order to avoid biasing. From the entire simulation period, a representative and geomagnetically quiet day 7 September 2013 has been chosen for the demonstration of the comparison results to analyze the affectivity of the model IRPE-TEC-121E and IRPE-TEC-121E(HWM) from geomagnetic crest station Hsinchu (24.80°N, 120.99°E geographic, magnetic dip 35.52°N). From the comparison, shown in the Figure 4a, it can be concluded that the model incorporated with neutral wind components (IRPE-TEC-121E(HWM)) shows better correspondence with actual VTEC than the ANN model without neutral wind components (IRPE-TEC-121E) except at diurnal maximum. IRI overestimates the VTEC values and henceforth shows maximum deviation from the VTEC almost throughout the day than other models. NeQuick shows better correspondence with actual VTEC along 121°E compared to 77°E and 88°E. On 7 September 2013, the deviations obtained from IRPE-TEC-121E, PIM, IRPE-TEC-121E(HWM), NeQuick, and IRI at diurnal peak VTEC are 0.3, 5, 2, 4, and 16 TECU, respectively. These results are tabulated in Table 4. The same comparisons have been done for April and September 2012 and April and September 2013.

The deviations of predicted VTEC from the actual VTEC have also been computed for IRPE-TEC-121E, PIM, IRPE-TEC-121E(HWM) NeQuick, and IRI for all geomagnetic quiet days of the entire month of September 2013 from Hsinchu (24.80°N, 120.99°E geographic, magnetic dip 35.52°N) for an elevation angle over 50°. Figure 4b shows the hourly median error analysis for all the models tested here in diurnal basis for the month of September 2013 along the EIA crest station Hsinchu. From Figure 4b, it can be established that PIM has shown maximum error before diurnal peak and IRI has shown maximum error after diurnal peak of TEC. The inclusion of neutral wind produces significant improvement in the prediction of the VTEC by generating less median error almost throughout the day. The maximum median error evaluated from IRPE-TEC-121E, PIM, IRPE-TEC-121E(HWM), NeQuick, and IRI are found to be 21, 27, 8, 20, and 22 TECU during 10:00 UT, 03:00 UT, 10:00 UT, 09:00 UT, and 10:00 UT, respectively, throughout the entire September 2013. These results are shown in Table 4. The corresponding universal time is shown after the median TEC values. The median errors obtained by all models at diurnal peak for September 2013 at Hsinchu are also tabulated in Table 4. However, the latitudinal variation of TEC along 121°E for a fixed time cannot be computed from those models due to the absence of any IGS station between 15°N and 24°N.

7. TEC Variation With Longitudinally Separated Artificial Neural-Network Based Models

After observing the applicability and improved performance of the three ANN-based TEC models coupled with the neutral horizontal wind components in the three different longitudinal sectors covering a wide

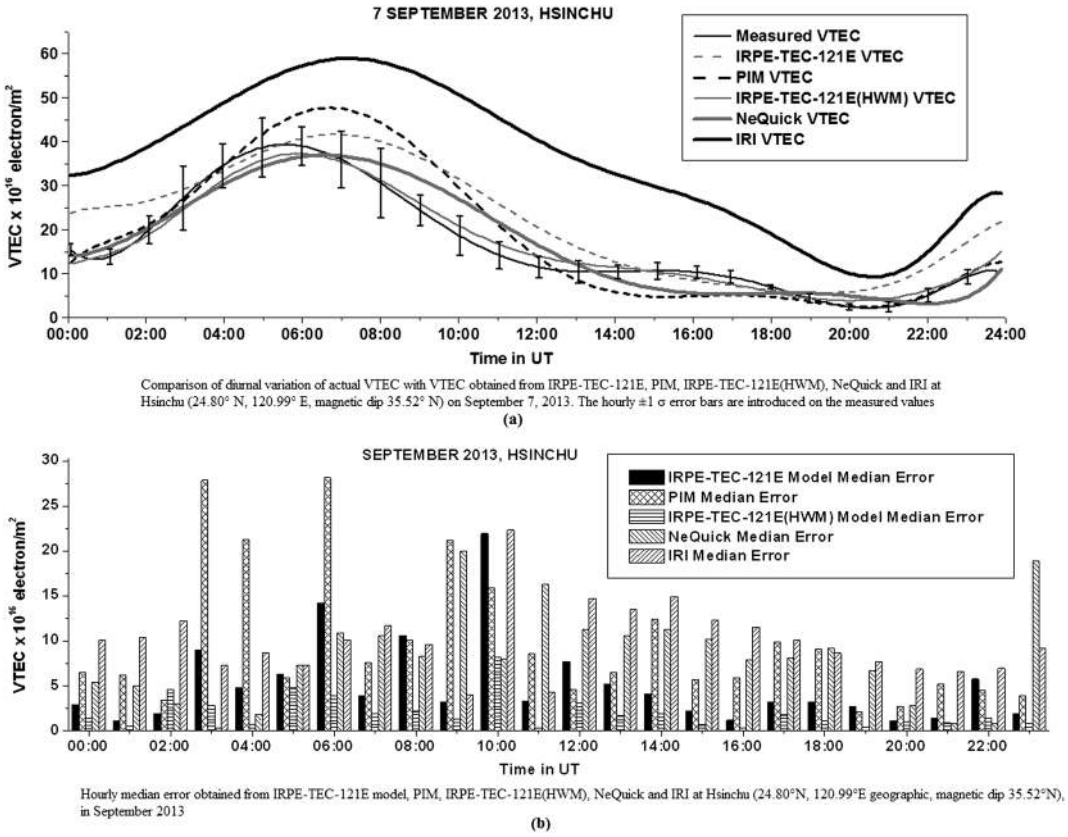

Figure 4. (a) Comparison of diurnal variation of actual VTEC with VTEC obtained from IRPE-TEC-121E, PIM, IRPE-TEC-121E (HWM), NeQuick, and IRI at Hsinchu (24.80°N, 120.99°E, magnetic dip 35.52°N) on 7 September 2013. The hourly ±1σ error bars are introduced on the measured values. (b) Hourly median error obtained from IRPE-TEC-121E model, PIM, IRPE-TEC-121E (HWM), NeQuick, and IRI at Hsinchu (24.80°N, 120.99°E geographic, magnetic dip 35.52°N) in September 2013.

latitudinal variation in this geophysically sensitive equatorial region, predictions from these models can be utilized to analyze any longitudinal variation in TEC after eliminating the effect from solar terminator. As the models IRPE-TEC-77E(HWM) and IRPE-TEC-121E(HWM) have shown good correspondence with the actual VTEC for the low-latitude regions along longitudes 77°E and 121°E, respectively, reliable TEC variation analysis along two distinct longitudes can be done using the predictions from these models. Two equinoctial months April 2013 and September 2013 have been utilized to generate the predictions of VTEC along 77°E and 121°E longitudes using IRPE-TEC-77E(HWM) and IRPE-TEC-121E(HWM), respectively, for geomagnetically quiet days (days with $Dst \geq -50$ nT). A representative geomagnetic quiet day from each equinoctial month (3 April 2013 and 8 September 2013) has been chosen to show longitudinal TEC variation removing the solar terminator effect. Two stations, Bhopal (23.28°N, 77.34°E geographic, magnetic dip 33.95°N) and Hsinchu (24.80°N, 120.99°E geographic, magnetic dip 35.52°N), have been chosen for the comparison as they are positioned along similar geomagnetic dip and almost the same latitude but in different longitudes (77°E and 121°E, respectively) and different geomagnetic declination angle (0° geomagnetic declination for Bhopal and 4°W for Hsinchu). The geographic locations of these two stations have been shown in Figure 1d. Thus, the latitudinal difference between these two stations can be assumed negligible. Both stations are situated on the EIA crest and have a wide longitudinal difference. TECs for April 2013 and September 2013 at Bhopal are computed from IRPE-TEC-77E(HWM), and TECs for Hsinchu for the same period are computed with IRPE-TEC-121E(HWM). Predicted VTECs from two geomagnetically quiet days each from April and September (3 April 2013 and 8 September 2013) corresponding models along 77°E and 121°E longitudes have been demonstrated in Figures 5a and 5b, respectively for elevation angle over 50°. From the figures, the conclusion can be easily derived that the TEC from Bhopal at 77°E is slightly higher than the TEC from Hsinchu at 121°E for most parts of the day. Now from the analysis of equation (3), the longitudinal TEC variation can be attributed to the variable recombination rate in varying longitudes. The

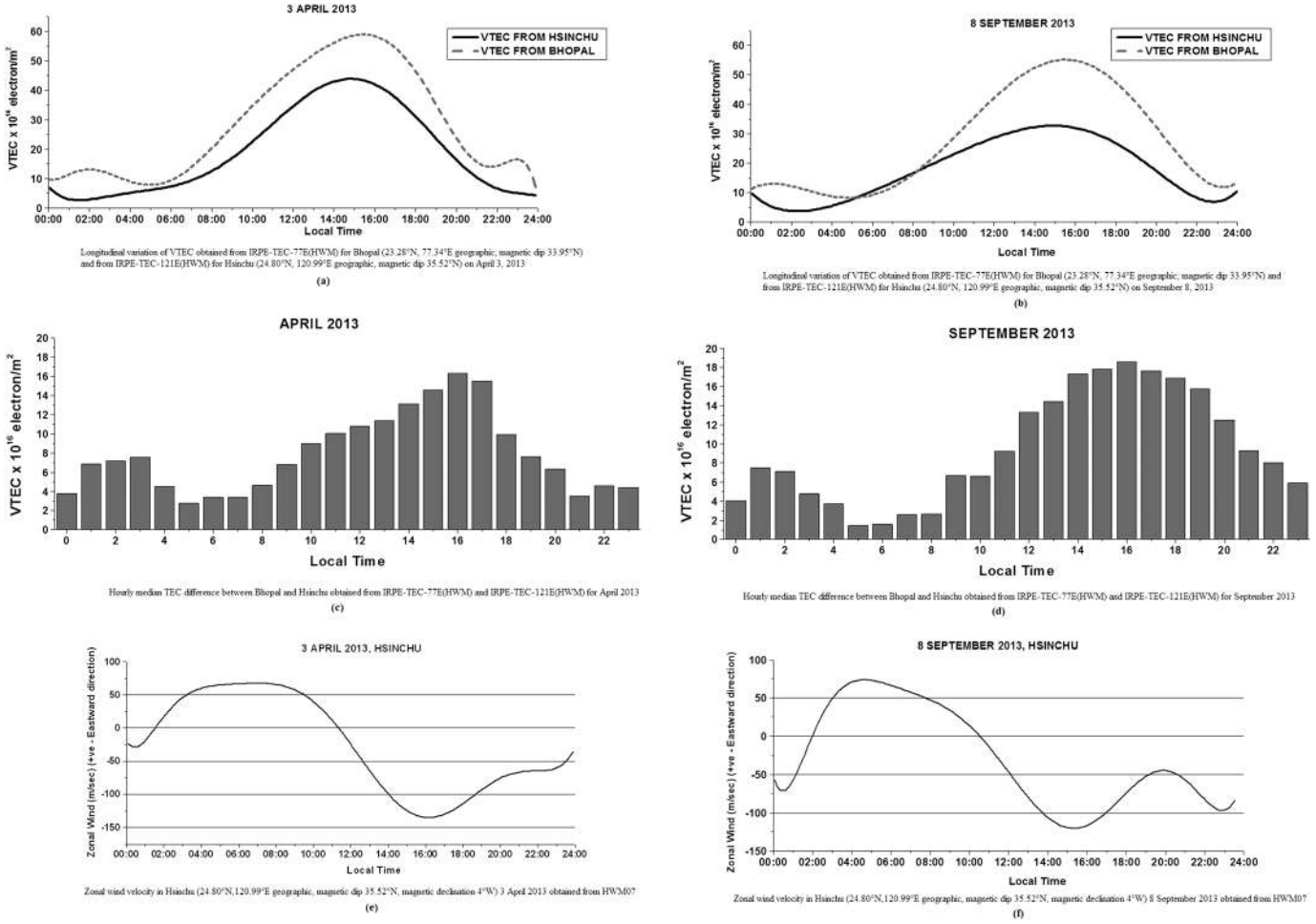

Figure 5. (a) Longitudinal variation of VTEC obtained from IRPE-TEC-77E(HWM) for Bhopal (23.28°N, 77.34°E geographic, magnetic dip 33.95°N) and from IRPE-TEC-121E(HWM) for Hsinchu (24.80°N, 120.99°E geographic, magnetic dip 35.52°N) on 3 April 2013. (b) Longitudinal variation of VTEC obtained from IRPE-TEC-77E(HWM) for Bhopal (23.28°N, 77.34°E geographic, magnetic dip 33.95°N) and from IRPE-TEC-121E(HWM) for Hsinchu (24.80°N, 120.99°E geographic, magnetic dip 35.52°N) on 8 September 2013. (c) Hourly median TEC differences between Bhopal and Hsinchu obtained from IRPE-TEC-77E(HWM) and IRPE-TEC-121E(HWM) for April 2013. (d) Hourly median TEC difference between Bhopal and Hsinchu obtained from IRPE-TEC-77E(HWM) and IRPE-TEC-121E(HWM) for September 2013. (e) Zonal wind velocity in Hsinchu (24.80°N, 120.99°E geographic, magnetic dip 35.52°N, magnetic declination 4°W) on 3 April 2013 obtained from HWM07. (f) Zonal wind velocity in Hsinchu (24.80°N,120.99°E geographic, magnetic dip 35.52°N, magnetic declination 4°W) on 8 September 2013 obtained from HWM07.

ion recombination rate depends on the magnetic field-aligned ion drift velocity *V*, which in turn depends on the variation of geomagnetic inclination angle, declination angle, and the zonal wind. As both the stations have almost the same geomagnetic inclination, the variation of TEC between these two stations can be attributed toward the variation of declination angle and the zonal wind only. The station Bhopal has been situated on the agonic line, and Hsinchu has been situated at slightly east from the agonic line in 2013, as shown in Figure 1d. As the station Bhopal almost situated on the agonic line, so its geomagnetic declination angle is almost zero. According to equation (3), the ion drift velocity at Bhopal is close to zero. Hence, the recombination rate does not depend on the zonal wind velocity and directions. Magnetic inclination angle is almost the same for both stations, and the sign should be positive as the inclination angles for those two stations are magnetic north. Hsinchu is situated on 4°W declination angle. According to equation (3), the conventional sign for a declination angle due west is negative. Another parameter which influences on vertical ion drift is the magnitude and direction for zonal wind. Zonal winds at Hsinchu for the corresponding days are computed from HWM07 model, and the variation of zonal wind along the local time for Hsinchu for 3 April 2013 and 8 September 2013 are shown in Figures 5e and 5f, respectively. From the diurnal variation of zonal wind, it can be observed that for most parts of the day, especially after 09:00 LT (local time), the direction of zonal wind is westward. So the direction sign should be negative. So at Hsinchu,

Table 5. Diurnal Comparison of TEC Between Two Longitudinally Separated Locations Bhopal and Hsinchu for April 2013 and September 2013

	Vernal Equinox (April 2013)				Autumnal Equinox (September 2013)			
	14:00–17:00 LT		05:00–08:00 LT		14:00–17:00 LT		05:00-08:00 LT	
	3 April 2013	Entire April 2013	3 April 2013	Entire April 2013	8 September 2013	Entire September 2013	8 September 2013	Entire September 2013
TEC difference between Bhopal and Hsinchu (TECU) (median TECU difference for the entire month)	13–17	13.14–16.32	1.5–7	2.79–4.63	20–23	17.34–18.59	0–2	1.44–2.67
Zonal wind speed at Hsinchu (m/s)	103–134 (westward)	99–148 (westward)	65–68 (eastward)	48–88 (eastward)	100–120 (westward)	96–121 (westward)	49–73 (eastward)	47–79 (eastward)

for a negative zonal wind, positive inclination angle and negative declination angle, the direction of ion drift should be negative or downward as it is computed from equation (3). The downward ion drift causes larger recombination rate. This can be attributed to the main possible reason to the lesser values of TEC at Hsinchu than Bhopal. Bhopal is situated on the agonic line, and hence, the vertical ion drift at Bhopal can be assumed to be on the order of the magnitude which is less significant than that of Hsinchu. From Figures 5a and 5b, it can be found that the longitudinal TEC differences between these two stations are maximized during the post-diurnal-peak hours around 14:00–17:00 LT. The longitudinal TEC differences between these two stations along 14:00–17:00 LT are observed to be 13–17 TECU during the entire 3 April 2013 and 20–23 TECU during 8 September 2013. The reason for this steep TEC differences can probably be explained by the maximum downward magnetic ion drift velocity at Hsinchu, which helps slight increment ion recombination rate. This maximum downward ion drift occurred due to maximum westward zonal wind flow along 14:00–17:00 LT in Hsinchu, where geomagnetic declination angle is west and inclination angle is north. From Figures 5e and 5f, it can be seen that zonal wind flow direction at Hsinchu becomes maximum westward during 14:00–17:00 LT (103–134 m/s westward at 3 April 2013 and around 100–120 m/s westward at 8 September 2013). This westward zonal wind causes highly downward ion drift for Hsinchu (west declination angle and north inclination angle) according to equation (3) reported by *Zhang et al*. [2011]. This downward ion drift increases higher recombination rate, and this prevents very high TEC value at Hsinchu during the diurnal peak time and post-diurnal-peak time of 14:00–17:00 LT, thus causing large TEC differences around 14:00–17:00 LT between Bhopal and Hsinchu. Similarly, from Figures 5a and 5b, the minimum TEC differences between the two stations can be seen around 05:00–08:00 LT. The longitudinal TEC differences during 05:00–08:00 LT are 1.5–7 TECU on 3 April 2013 and 0–2 TECU on 8 September 2013. On 8 September 2013 at 05:00–08:00 LT, the TEC at Bhopal is observed to be less than the TEC of Hsinchu for 05:00–08:00 LT. This may be explained in terms of upward ion drift velocity at Hsinchu due to the eastward zonal wind flow. From Figures 5e and 5f, the zonal wind speed at Hsinchu during around 05:00–08:00 LT becomes maximum eastward with a speed of 65–68 m/s on 3 April 2013 and 49–73 m/s on 8 September 2013. This highly eastward zonal wind produces upward ion drift for Hsinchu (west declination angle and north inclination angle) according to equation (3), causing less recombination rate and thus increasing the TEC value at Hsinchu. Thus, the net difference in TEC value between Bhopal and Hsinchu becomes least at 05:00–08:00 LT than the rest of the day. The similar comparisons have been done for all the geomagnetically quiet days from April 2013 and September 2013. The least TEC differences between Bhopal and Hsinchu during 05:00–08:00 LT may also be attributed to low values of TEC around 05:00 LT in both stations. For all other geomagnetically quiet days of April 2013 and September 2013, the TEC differences between Bhopal and Hsinchu are found to be maximum around 14:00–17:00 LT and minimum around 05:00–08:00 LT. The diurnal variations of TEC differences between these two stations for all geomagnetic quiet days from entire April 2013 and September 2013 have been performed, and the results summarized alongside 3 April 2013 and 8 September 2013 are shown in Table 5. The median TEC differences between Bhopal and Hsinchu per hour are computed from ANN model simulations, and these results are displayed in Figures 5c and 5d. The results are shown in Table 5. During 14:00–17:00 LT, the median TEC differences between Bhopal and Hsinchu are observed to be maximum (13.14–16.32 TECU for April 2013 and 17.34–18.59 TECU for September 2013). The minimum median TEC differences along these two stations are obtained during 05:00–08:00 LT (2.79–4.63 TECU for April 2013 and 1.44–2.67 TECU for September 2013). In April 2013, the longitudinal TEC differences get considerably reduced during another time interval of 21:00–23:00 LT also (3.51–4.43 TECU).

8. Conclusions and Discussions

Transionospheric radio signals from spacecraft and navigation satellites are always attenuated by the TEC present in the ionospheric medium. For reliable operations of transionospheric radio signals, high accuracy is required in TEC prediction. Standard midlatitude models like IRI, NeQuick, and PIM are incapable of predicting the TEC in the dynamic equatorial region. The prediction variations are smoothed in nature for these models which makes them unable to present good correspondence with the actual VTEC in this region [*Paul et al*., 2005; *Bhuyan and Borah*, 2007]. This initiates the necessity of an ANN-based TEC model designed with database of real-time local TEC data.

The existence of longitudinal TEC differences has already been reported in *Su et al*. [1996] and *Zhang et al*. [2011]. To observe any longitudinal difference in TEC in low-latitude region, three ANN-based TEC prediction models have been developed along three separate longitudes in the equatorial region. The present manuscript reports the development and performance of the three ANN-based TEC models: (i) IRPE-TEC-88E using real-time GPS data for the duration from 1 January 2007 to 15 September 2011 along the longitude of 88°E, (ii) IRPE-TEC-77E using real-time GAGAN GPS data for the duration of January 2004 to March 2005 along the longitude of 77°E, and (iii) IRPE-TEC-121E with real-time GPS data spanning the period of January 2011 to March 2012 along the longitude 121°E along the low-latitude regions. The relation between neutral wind velocities and TEC has already been reported [*Balan et al*., 2009]. For this reason, these currently developed ANN-based models are further upgraded with the inclusion of neutral winds (meridional wind and zonal wind) as model inputs to make the predictions from the models more accurate. The newly developed models along 88°E, 77°E, and 121°E (IRPE-TEC-88E(HWM), IRPE-TEC-77E(HWM), and IRPE-TEC-121E(HWM), respectively) have been compared with the neural network models without the incorporation of neutral winds. The outputs of neutral wind-incorporated ANN models are proven to be more in correspondence with the diurnal as well as the latitudinal variation of actual VTEC than the ANN models without the neutral wind components as inputs and other standard models like NeQuick, PIM, and IRI. These reinforce that neutral wind plays an important role in determining TEC.

From the analysis, it can be summarized that neutral wind coupled ANN models have shown better correspondence with the actual VTEC than the rest of the models simulated. These conclusions validate the incorporation of neutral winds as TEC model inputs for better and accurate predictions. Empirical models like PIM, NeQuick, and IRI constitute midlatitude region and American and European longitude sector TEC data and hence produce large deviation from measured TEC at equatorial regions [*Paul et al*., 2005; *Bhuyan and Borah*, 2007]. The smoothed prediction nature of these models makes them unable to properly describe the wide and dynamic diurnal and spatial variations of TEC in this equatorial region. Electrodynamic drift parameters used in these models are averaged over their prolonged database, and this is the reason why these models are unable to properly describe the dynamic equatorial plasma transport process. For accurate prediction of this sharp diurnal, spatial and the day-to-day variation of TEC in this low-latitude region, real-time local TEC data set-based model is required. The currently developed ANN models are generated by local TEC data. The predictions from these models show better correspondence with low-latitude TEC variation. Thus, these IRPE-TEC models coupled with neutral wind inputs along low latitudes could provide the initiative for accurate TEC prediction, which is essential for SBAS.

The improved prediction of the neutral wind-included neural network-based real-time TEC models over the standard models like PIM, NeQuick, and IRI has been proved now by a chain of simulation during equinoctial periods. In this regard, these longitudinally separated neural network-based TEC models, IRPE-TEC-77E(HWM) and IRPE-TEC-121E(HWM), designed along the longitudes of 77°E and 121°E, respectively, can be used to observe any longitudinal differences present in the diurnal distribution of TEC except the difference due to solar terminator. The comparisons from the local time-predicted diurnal VTEC values along 77°E and 121°E obtained from those models for all geomagnetically quiet days (days with $Dst \geq -50$ nT) of April and September 2013 have been analyzed with the variations of the zonal wind through the regions. Two almost equal geomagnetic dip and the same latitude stations, Bhopal (23.28°N, 77.34°E geographic, magnetic dip 33.95°N) and Hsinchu (24.80°N, 120.99°E geographic, magnetic dip 35.52°N), are chosen to perform the comparisons for geomagnetic quiet days along the two equinox months of April and September for the year 2013. Bhopal and Hsinchu are separated by different geographic longitudes (77°E and 121°E, respectively) and geomagnetic declination angles (0° geomagnetic declination for Bhopal and 4°W for Hsinchu). TECs for

Bhopal are computed from IRPE-TEC-77E(HWM), and TECs for Hsinchu are computed with IRPE-TEC-121E(HWM). After eliminating the solar terminator effect, VTEC at Bhopal appears to be higher than the VTEC of Hsinchu almost throughout the day, especially at the diurnal peak (Table 5). This VTEC variation through the longitude separation between these two stations may be explained by the relation of TEC with the zonal wind of the region as well as with the inclination and declination angles of the station as reported in the literatures by *Su et al.* [1996] and *Zhang et al.* [2011]. This explanation is elaborated in section 7. This can be a suitable explanation for the longitudinal variability of TEC along the low latitudes. This also reinforces the dependency of TEC over the geomagnetic inclination and declination angles and the zonal wind components. The longitudinal differences of TEC values over two longitudinally separated stations also vary diurnally, and it is confirmed by the computations of TEC from ANN-based real-time-data-driven models for April and September 2013 (Figures 5c and 5d and Table 5) after eliminating the solar terminator effect. The maximum longitudinal TEC differences between Bhopal and Hsinchu are obtained during 14:00–17:00 LT and the minimum longitudinal TEC differences during 05:00–08:00 LT for April and September 2013. The possible explanation for this diurnal variation is given in section 7 with the help of zonal wind and declination angle as well as inclination angle for those stations. Thus, neural network-based model TEC computation technique along the different longitudes reported in this literature allowed to generate the clear picture of the longitudinal TEC variations along the low latitudes and their dependency over zonal wind and geomagnetic inclination and declination angles. From the neural network-based TEC model analysis, it can also be shown that these longitudinal TEC differences between different longitude stations also suffer diurnal variation, and these variations can be explained by the variation of zonal wind. So these longitudinally separated ANN-based real-time TEC model technique can be an important tool to generate detailed picture about longitudinal variation of TEC along low latitudes.

Acknowledgments

The authors acknowledge the Indian Space Research Organization (ISRO) for supporting this work through research projects at the S. K. Mitra Centre for Research in Space Environment, University of Calcutta, Calcutta, India. The GAGAN data for the period of 2004–2005 have been made available by ISRO and Airport Authority of India. The authors acknowledge the Asian Office of Aerospace Research and Development for providing the SCINDA data. The model International Reference Ionosphere (IRI 2007) is available at the website http://omniweb.gsfc.nasa.gov/vitmo/iri_vitmo.html. The authors also acknowledge R. Daniell of the Computational Physics, Incorporated, Waltham, Massachusetts, for making the PIM model (PIM 1.7) available. Authors sincerely thank Aeronomy and Radiopropagation Laboratory of the Abdus Salam International Centre for Theoretical Physics Trieste, Italy, for providing the NeQuick model. The IGS data set, which is used to design for IRPE-TEC-121E and IRPE-TEC-121E(HWM), was obtained from the website http://sopac.ucsd.edu/. The authors would like to thank (i) S. Roy and K. Basu of the K. N. College, Baharampore, India, for providing the data from Baharampore GPS receiver, (ii) S. Halder of North Bengal University, Siliguri, India, for providing the GPS data from North Bengal University, Siliguri, India, and (iii) Bharat Sevashram Sangha, Farakka, India, for providing the GPS data from Farakka, India.

Alan Rodger thanks the reviewers for their assistance in evaluating this paper.

References

Alken, P., S. Maus, J. Emmert, and D. P. Drob (2008), Improved horizontal wind model HWM07 enables estimation of equatorial ionospheric electric fields from satellite magnetic measurements, *Geophys. Res. Lett.*, *35*, L11105, doi:10.1029/2008GL033580.

Altinay, O., E. Tulunay, and Y. Tulunay (1997), Forecasting of ionospheric critical frequency using neural networks, *Geophys. Res. Lett.*, *24*(12), 1467–1470, doi:10.1029/97GL01381.

Appleton, E. V. (1946), Two anomalies in the ionosphere, *Nature*, *157*(3995), 691–693, doi:10.1038/157691a0.

Balan, N., H. Alleyne, Y. Otsuka, D. V. Lekshmi, B. G. Fejer, and I. McCrea (2009), Relative effects of electric field and neutral wind on positive ionospheric storms, *Earth, Planets Space*, *61*(4), 439–445.

Bhuyan, P. K., and R. R. Borah (2007), TEC derived from GPS network in India and comparison with the IRI, *Adv. Space Res.*, *39*(5), 830–840, doi:10.1016/j.asr.2006.12.042.

Breed, A. M., G. L. Goodwin, A. M. Vandenberg, E. A. Essex, K. J. W. Lynn, and J. H. Silby (1997), Ionospheric total electron content and slab thickness determined in Australia, *Radio Sci.*, *32*(4), 1635–1643, doi:10.1029/97RS00454.

Daniell, R. E., Jr., L. D. Brown, D. N. Anderson, M. W. Fox, P. H. Doherty, D. T. Decker, J. J. Sojka, and R. W. Schunk (1995), Parameterized ionospheric model: A global ionospheric parameterization based on first principles models, *Radio Sci.*, *30*(5), 1499–1510, doi:10.1029/95RS01826.

di Giovanni, G., and S. M. Radicella (1990), An Analytical Model of the electron density profile in the ionosphere, *Adv. Space Res.*, *10*(11), 27–30, doi:10.1016/0273-1177(90)90301-F.

Drob, D. P., et al. (2008), An empirical model of the Earth's horizontal wind fields: HWM07, *J. Geophys. Res.*, *113*, A12304, doi:10.1029/2008JA013668.

Fesen, C. G., G. Crowley, and R. G. Roble (1989), Ionospheric effects at low latitudes during the March 22, 1979, geomagnetic storm, *J. Geophys. Res.*, *94*(A5), 5405–5417, doi:10.1029/JA094iA05p05405.

Hanson, W. B., and R. J. Moffett (1966), Ionization transport effects in the equatorial F region, *J. Geophys. Res.*, *71*(23), 5559–5572, doi:10.1029/JZ071i023p05559.

Hernandez-Pajares, M., J. M. Juan, and J. Sanz (1997), Neural network modeling of the ionospheric electron content at global scale using GPS data, *Radio Sci.*, *32*(3), 1081–1089, doi:10.1029/97RS00431.

Huang, Y., K. Cheng, and S. Chen (1989), On the equatorial anomaly of the ionospheric total electron content near the northern anomaly crest region, *J. Geophys. Res.*, *94*(A10), 13,515–13,525, doi:10.1029/JA094iA10p13515.

Kelley, M. C., M. N. Vlasov, J. C. Foster, and A. J. Coster (2004), A quantitative explanation for the phenomenon known as storm-enhanced density, *Geophys. Res. Lett.*, *31*, L19809, doi:10.1029/2004GL020875.

Klobuchar, J. A., P. H. Doherty, A. Das Gupta, M. R. Sivaraman, and A. D. Sarma (2001), Equatorial anomaly gradient effects on a space-based augmentation system Proc., *International Beacon Satellite Symposium*, *Boston* (*USA*).

Kumluca, A., E. Tulunay, I. Topalli, and Y. Tulunay (1999), Temporal and spatial forecasting of ionospheric critical frequency using neural networks, *Radio Sci.*, *34*(6), 1497–1506, doi:10.1029/1999RS900070.

Leandro, R. F. (2004), A new technique to TEC regional modeling using a neural network, in *Proceedings of the ION GNSS 2004*, *Long Beach*, *California*, 20–21 September, Inst. of Navig., Fairfax, Va.

Leandro, R. F., and M. C. Santos (2007), A neural network approach for regional vertical total electron content modeling, *Stud. Geophys. Geod.*, *51*(2), 279–292, doi:10.1007/s11200-007-0015-6.

Marquez, L., and T. Hill (1992), Function approximation using back-propagation and general regression neural networks, in *Proceedings of the Twenty-Sixth Hawaii International Conference on System Sciences*, vol. 4, pp. 607–615, IEEE Press, Piscataway, N. J.

McKinnell, L. A., and A. W. V. Poole (2001), Ionospheric variability and electron density profile studies with neural networks, *Adv. Space Res.*, *27*(1), 83–90, doi:10.1016/S0273-1177(00)00142-3.

Nava, B., S. M. Radicella, R. Leitinger, and P. Coïsson (2007), Use of total electron content data to analyze ionosphere electron density gradients, *Adv. Space Res.*, *39*(8), 1292–1297, doi:10.1016/j.asr.2007.01.041.

Oyeyemi, E. O., A. W. V. Poole, and L. A. McKinnell (2005a), On the global model for f_oF_2 using neural networks, *Radio Sci.*, *40*, RS6011, doi:10.1029/2004RS003223.

Oyeyemi, E. O., A. W. V. Poole, and L. A. McKinnell (2005b), On the global short-term forecasting of the ionospheric critical frequency f_oF_2 up to 5 hours in advance using neural networks, *Radio Sci.*, *40*, RS6012, doi:10.1029/2004RS003239.

Oyeyemi, E. O., L. A. McKinnell, and A. W. V. Poole (2006), Near-real time foF2 predictions using neural networks, *J. Atmos. Sol. Terr. Phys.*, *68*(16), 1807–1818, doi:10.1016/j.jastp.2006.07.002.

Paul, A., S. K. Chakraborty, A. Das, and A. Dasgupta (2005), Estimation of satellite-based augmentation system grid size at low latitudes in the Indian zone, *Navigation: J. Inst. Navig.*, *52*(1), 15–22.

Paul, A., A. Das, and A. DasGupta (2011), Characteristics of SBAS grid sizes around the northern crest of the equatorial ionization anomaly, *J. Atmos. Sol. Terr. Phys.*, *73*(13), 1715–1722.

Radicella, S. M. (2009), The NeQuick model genesis, uses and evaluation, *Ann. Geophys.*, *52*(3/4), 417–422, doi:10.4401/ag-4597.

Rastogi, R. G., and J. A. Klobuchar (1990), Ionospheric electron content within the equatorial F_2 layer anomaly belt, *J. Geophys. Res.*, *95*(A11), 19,045–19,052, doi:10.1029/JA095iA11p19045.

Rawer, K., and D. Bilitza (1989), Electron density profile description in the international reference ionosphere, *J. Atmos. Terr. Phys.*, *51*(9–10), 781–790, doi:10.1016/0021-9169(89)90035-4.

Rawer, K., and D. Bilitza (1990), International reference ionosphere-plasma densities: Status 1988, *Adv. Space Res.*, *10*(8), 5–14, doi:10.1016/0273-1177(90)90177-2.

Seemala, G. K., and C. E. Valladares (2011), Statistics of total electron content depletions observed over the South American continent for the year 2008, *Radio Sci.*, *46*, RS5019, doi:10.1029/2011RS004722.

Senalp, E. T., E. Tulunay, and Y. Tulunay (2008), Total electron content (TEC) forecasting by cascade modeling: A possible alternative to the IRI-2001, *Radio Sci.*, *43*, RS4016, doi:10.1029/2007RS003719.

Su, Y. Z., K. I. Oyama, G. J. Bailey, S. Fukao, T. Takahashi, and H. Oya (1996), Longitudinal variations of the topside ionosphere at low latitudes: Satellite measurements and mathematical modelings, *J. Geophys. Res.*, *101*(A8), 17,191–17,205, doi:10.1029/96JA01315.

Sur, D., and A. Paul (2013), Comparison of standard TEC models with a neural network based TEC model using multistation GPS TEC around the northern crest of equatorial ionization anomaly in the Indian longitude sector during the low and moderate solar activity levels of the 24th solar cycle, *Adv. Space Res.*, *52*(5), 810–820, doi:10.1016/j.asr.2013.05.020.

Tulunay, E., E. T. Senalp, S. M. Radicella, and Y. Tulunay (2006), Forecasting total electron content maps by neural network technique, *Radio Sci.*, *41*, RS4016, doi:10.1029/2005RS003285.

Wintoft, P., and L. R. Cander (1999), Short-term prediction of foF2 using time-delay neural network, *Phys. Chem. Earth(C)*, *24*(4), 343–347, doi:10.1016/S1464-1917(99)00009-4.

Yilmaz, A., K. E. Akdogan, and M. Gurun (2009), Regional TEC mapping using neural networks, *Radio Sci.*, *44*, RS3007, doi:10.1029/2008RS004049.

Zhang, S., J. C. Foster, A. J. Coster, and P. J. Erickson (2011), East-west coast differences in total electron content over the continental U.S., *Geophys. Res. Lett.*, *38*, L19101, doi:10.1029/2011GL049116.